JOURNAL OF MATERIALS SCIENCE **38** (2003) 331 – 337

Antiphase domain morphologies in Ti_3Al-Si alloys

A. JAZAYERI-G
Institute for Technology Development Research, North of Sharif University of Technology, 14599, Tehran, Iran

R. A. BUCKLEY, H. A. DAVIES
Department of Engineering Materials, University of Sheffield, Sheffield, S1 3JD, UK
E-mail: r.a.buckley@sheffield.ac.uk

Ti_3Al based alloys with additions of Si, V, and V + Si were prepared in ingot form by argon arc co-melting and in the form of rapidly solidified ribbons by chill block melt spinning. Binary Ti_3Al and ternary Ti_3Al-Si arc-melted ingots showed equiaxed antiphase boundaries (APBs) in the α_2 (DO_{19}) grain interiors with columnar APBs adjacent to the grain boundaries. In the melt spun ribbons, which undergo high cooling rates, three types of antiphase domain (APD) morphologies (fine, columnar, and coarse equiaxed APDs) were observed in any single α_2 grain. Addition of 15 at.%V to these alloys led to retention of the ordered β (B2) phase with a relatively large antiphase domain size.

1. Introduction

Titanium aluminides based on Ti_3Al are attractive candidates for aerospace structural and engine applications because of their elevated temperature strength and low density [1]. These alloys exhibit ordered $\alpha_2(DO_{19}) + \beta(B2)$ structure. Many of the mechanical properties of ordered alloys have been interpreted on the basis of the presence of antiphase domains (APDs) and antiphase domain boundaries (APBs), and of their particular characteristics [2]. The mechanical strength is influenced by these features through their effects on the structure, generation and mobility of dislocations [3]. For example, the size of the APDs is an important factor in determining the yield strength of the Ti_3Al [4].

The effect of rapid solidification (R.S.) in samples subjected to high cooling rates, as well as promoting refined and more homogeneous microstructures, will modify the subsequent solid state transformations with the potential of refinement of APD sizes. The influence of R.S. on APD structures has previously received little attention. In this paper, the APD morphologies in Ti_3Al-Si and Ti_3Al-V-Si arc-melted ingots and in melt spun ribbons are briefly reported and discussed.

2. Experimental procedures

Ti_3Al based ingots with additions of Si, V, and Si + V were prepared from high purity elements by argon arc-melting. The nominal and chemically analysed compositions of the alloys are listed in Table I. Rapidly solidified ribbons were produced by chill block melt spinning the ingot material onto a copper roll at circumferential velocities in the range 15–40 m/s. The ribbon thickness varied correspondingly between 70 and 20 μm. The as-cast microstructures of ingots and ribbons were characterised using optical microscopy, SEM, SEM-EDX microanalysis, TEM and XRD.

3. Results

We have reported the microstructures of Ti_3Al-Si ingots and ribbons in detail elsewhere [5, 6]. In summary, addition of Si to Ti_3Al leads to two phase microstructures, consisting of α_2-Ti_3(Al,Si) matrix and ζ-Ti_5(Si,$Al)_3$ rods, formed via an eutectic reaction. Addition of 15 at.%V to Ti_3Al and ternary Ti_3Al-Si alloys leads to retention of the ordered β phase in place of α_2 at room temperature. V addition does not change the course of the eutectic reaction occurring in the ternary Ti_3Al-Si alloys and the solidification structure of the quaternary ingots consists of ζ-$(Ti,V)_5(Si,Al)_3$ rods embedded in the β-(Ti,V)(Al,Si) matrix phase.

3.1. Arc-melted ingots

3.1.1. Alloy A

The binary Ti-25 at.%Al alloy A showed a single phase, ordered α_2, grain structure in the as-cast condition. This phase contains fine APDs, as shown in Fig. 1. The APD structure showed a maze pattern with no preferential crystallographic orientation of APBs. However, adjacent to the grain boundaries, they had a columnar morphology perpendicular to the grain boundaries.

3.1.2. Alloy F

The Ti-25Al-15V(at.%) alloy F exhibited a single phase, ordered β, grain structure. A typical DF image of the ordered β-(Ti,V)Al phase is shown in Fig. 2. This phase contains relatively large antiphase domains. Such domains are characteristic of a high order-disorder transition temperature at which domain boundary mobility is high and hence domain coarsening is rapid.

3.1.3. Hypoeutectic alloys B and C

The solidification microstructures of the ingots of Ti-25Al-2.5Si(at.%) alloy B and Ti-25Al-5Si(at.%)

TABLE I Nominal composition and chemical analysis of the arc-melted ingots and of the melt-spun ribbons (at.%)

Alloy	Composition	Ti	Al	Si	V	O_2
A	Nominal composition	75	25	–	–	–
	Arc-melted ingot analysis	Bal.	25.2	0.21	–	0.21 (830 wppm)
	Melt-spun ribbon analysis	Bal.	24.1	1.96	–	2.7 (1.04 wt%)
B	Nominal composition	75	25	2.5	–	–
	Arc-melted ingot analysis	–	–	–	–	–
	Melt-spun ribbon analysis	Bal.	24.1	3.44	–	2.2 (0.84 wt%)
C	Nominal composition	70	25	5	–	–
	Arc-melted ingot analysis	Bal.	24.6	4.67	–	0.25 (960 wppm)
	Melt-spun ribbon analysis	Bal.	24.1	5.03	–	0.79 (0.31 wt%)
D	Nominal composition	67.5	25	7.5	–	–
	Arc-melted ingot analysis	Bal.	24.4	6.99	–	0.08 (240 wppm)
	Melt-spun ribbon analysis	Bal.	23.7	7.16	–	0.33 (0.13 wt%)
E	Nominal composition	65	25	10	–	–
	Arc-melted ingot analysis	Bal.	24.1	9.45	–	0.12 (500 wppm)
	Melt-spun ribbon analysis	Bal.	23.3	9.24	–	0.29 (0.11 wt%)
F	Nominal composition	60	25	–	15	
G	Nominal composition	55	25	5	15	
H	Nominal composition	52.5	25	7.5	15	

Figure 1 Alloy A, Ti-25at.%Al, as-cast in argon arc furnace; BF micrograph showing equiaxed APDs in the α_2-Ti_3Al grain interiors and columnar APDs perpendicular to the grain boundaries, $g = 001_{DO19}$.

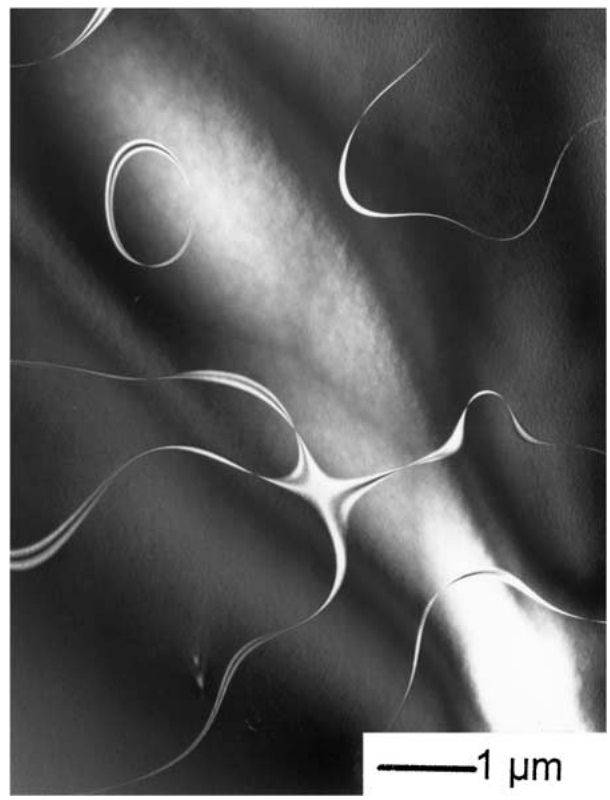

Figure 2 Alloy F, Ti-25Al-15V(at.%), as-cast in argon arc furnace showing large APDs in the ordered B2-(Ti,V)Al phase, TEM DF image on $(001)_{B2}$.

alloy C consisted of primary α_2-Ti_3(Al,Si) cells/dendrites with inter-cellular/-dendritic eutectic. BF and DF observations indicated that the α_2 cells/dendrites contained APBs, i.e. equiaxed APDs in the α_2 grain interiors and columnar APDs prependicular to the grain boundaries (Fig. 3a); these are similar to the APDs observed in alloy A. TEM examination of the eutectic mixture showed fine APBs in the α_2-Ti_3(Al,Si) matrix phase (Fig. 3b).

3.1.4. Eutectic alloy D

The Ti-25Al-7.5Si(at.%) alloy D exhibited cellular eutectic grains in the as-cast state. A typical DF image obtained with the $\alpha_2(101)$ superlattice reflection and showing fine APDs in the α_2 matrix phase, is illustrated in Fig. 4.

3.1.5. Hypereutectic alloy E

The as-cast Ti-25Al-10Si(at.%) alloy E consisted of large primary needles of ζ-$Ti_5(Si,Al)_3$ phase with the eutectic mixture of α_2 and ζ phases. TEM observations revealed that the α_2 matrix of this eutectic had the same equiaxed APD structure as the matrix phase in both the hypoeutectic alloy C and eutectic alloy D.

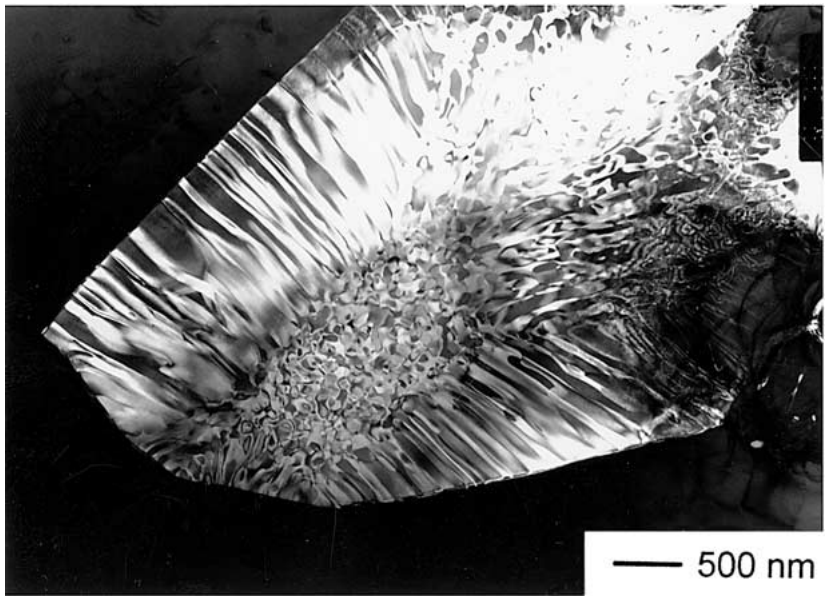

(a)

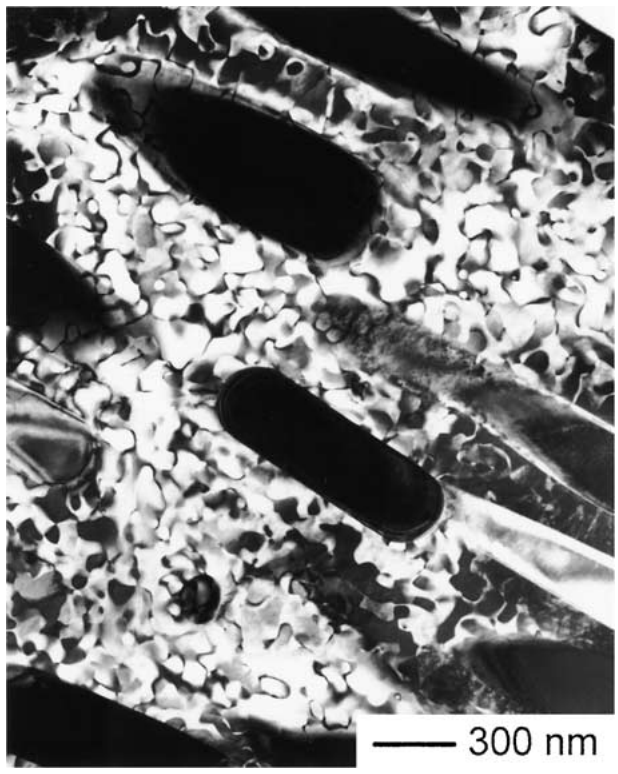

(b)

Figure 3 Different morphologies of APDs in the primary α_2-Ti_3(Al,Si) cells/dendrites; note columnar APDs perpendicular to the boundaries of the α_2 cells/dendrites, (a) Alloy B, and (b) Alloy C, both DF micrographs on $(010)_{DO19}$ showing APBs in the α_2-Ti_3(Al,Si) matrix phase of the eutectic mixture, TEM.

3.2. Melt-spun ribbons

3.2.1. Alloy A

One batch of melt-spun ribbon of alloy A exhibited single phase α_2 grains which contained three types of APD morphologies (Fig. 5). These morphologies were located in three distinct regions of the grains; (I) a zone of very fine APDs immediately adjacent to the grain boundaries, (II) a layer of columnar APDs, a little further from the boundaries and (III) a zone of coarse, equiaxed APDs in the grain interiors.

Another batch of melt-spun ribbon of alloy A exhibited α_2 grains which contained only two types of APD morphologies, i.e. equiaxed APBs in the grain interiors and columnar APBs adjacent to the grain boundaries (Fig. 6).

3.2.2. Hypoeutectic alloys B and C

TEM examination of ribbons of alloys B and C revealed a lath type of martensitic structure in the primary α_2-Ti_3(Al,Si) cells/dendrites [6]. Three types of antiphase domain morphologies (fine, columnar, and coarse equiaxed APDs) were observed in the α_2 cells/dendrites of ribbon B (Fig. 7a), the same morphologies as those in the α_2-Ti_3Al grains of ribbons of

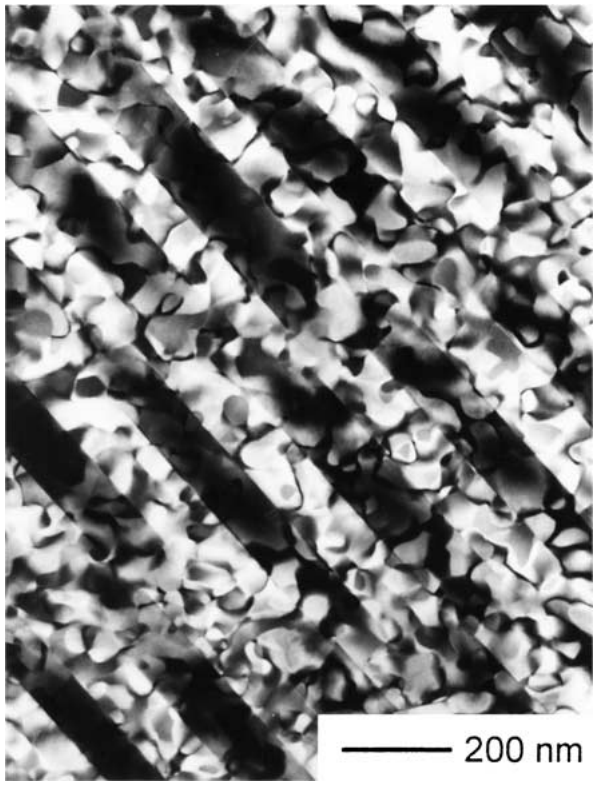

Figure 4 Alloy D, Ti-25Al-7.5Si (at.%), as-cast in argon arc furnace; DF image obtained with $\alpha_2(101)$ superlattice reflection, showing APBs in the α_2-$Ti_3(Al,Si)$ matrix of the eutectic, TEM.

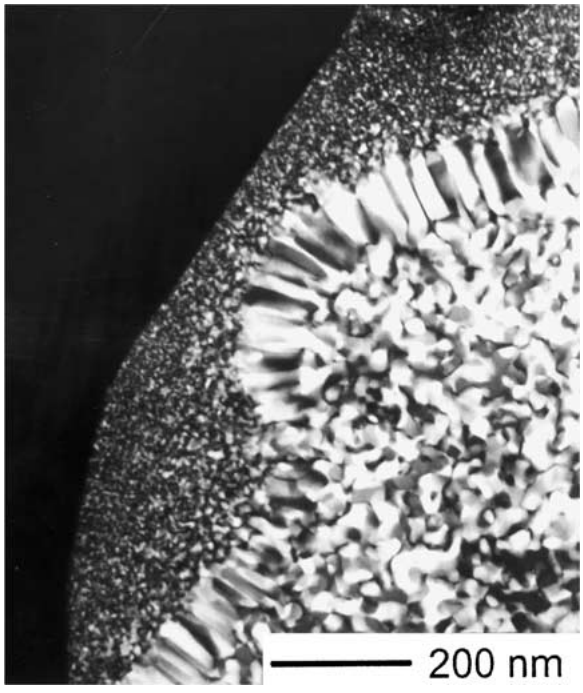

Figure 5 Ti-25 at.%Al, melt spun at 25 m/s. Three different morphologies of APDs in the α_2 grains, i.e. fine, columnar, and coarse equiaxed APDs, DF image on $(101)_{DO19}$, TEM.

alloy A. The primary dendrites in ribbon C consisted of only very fine APBs (Fig. 7b).

3.2.3. Hypoeutectic alloy G

Melt-spun ribbon of alloy G exhibited primary β-(Ti,V)(Al,Si) dendrites with interdendritic ζ-$(Ti,V)_5(Si,Al)_3$ phase (Fig. 8a). BF and DF images taken from a B2(100) superlattice reflection indicated that the primary dendrites contained relatively large APBs, as shown in Fig. 8b.

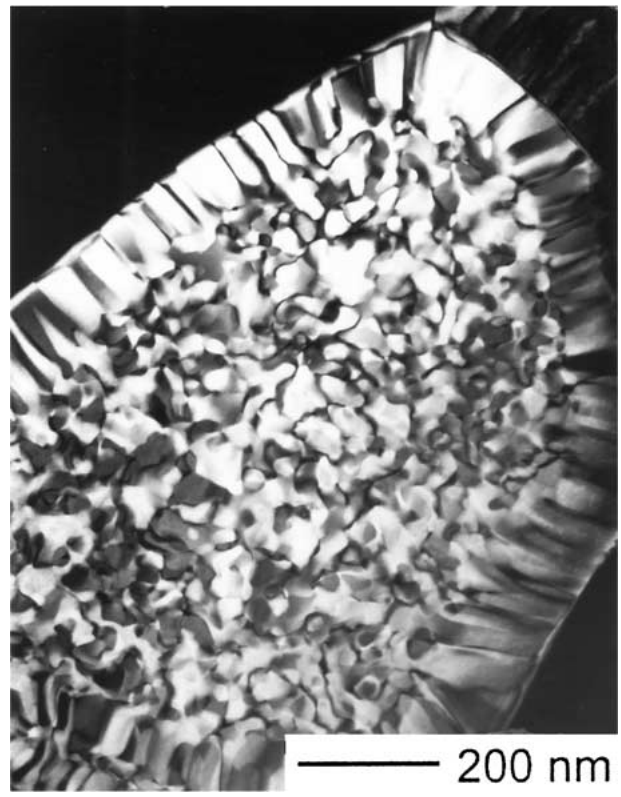

Figure 6 Ti-25 at.%Al, melt spun at 30 m/s; DF image on $(101)_{DO19}$, showing columnar APDs adjacent to the α_2-grain boundaries and equiaxed APDs in the grain interiors, TEM.

3.2.4. Eutectic alloy D

Ribbon of eutectic alloy D, melt spun at higher roll speeds, i.e. at very high rates of cooling, exhibited a hypoeutectic structure, i.e. primary α_2 dendrites with interdendritic ζ phase (Fig. 9a). A martensitic structure was observed in the α_2 dendrites; a DF image taken with $\alpha_2(101)$ superlattice reflection showed very fine APDs in these dendrites (Fig. 9b). Close to the free surface of the ribbons, where the cooling rate was slower, the eutectic structure was observed. X-ray diffraction analysis and TEM observations revealed the existence of the B2 phase in the matrix phase of this eutectic mixture [6].

3.2.5. Eutectic alloy H

Ribbon of alloy H melt-spun at a roll speed of 30 m/s exhibited a hypoeutectic structure consisting of the primary β-(Ti,V)(Al,Si) dendrites with interdendritic ζ-$(Ti,V)_5(Si,Al)_3$ phase. The primary β dendrites contained large antiphase domains (Fig. 10). The antiphase domains observed are an indication of the high ordering temperature of the β phase and/or rapid APB mobility.

4. Discussion

α_2-Ti_3Al grains and primary α_2-$Ti_3(Al,Si)$ cells/dendrites in the arc-melted ingots exhibited equiaxed APDs, with no preferential crystallographic orientation in the grain interiors and columnar APDs

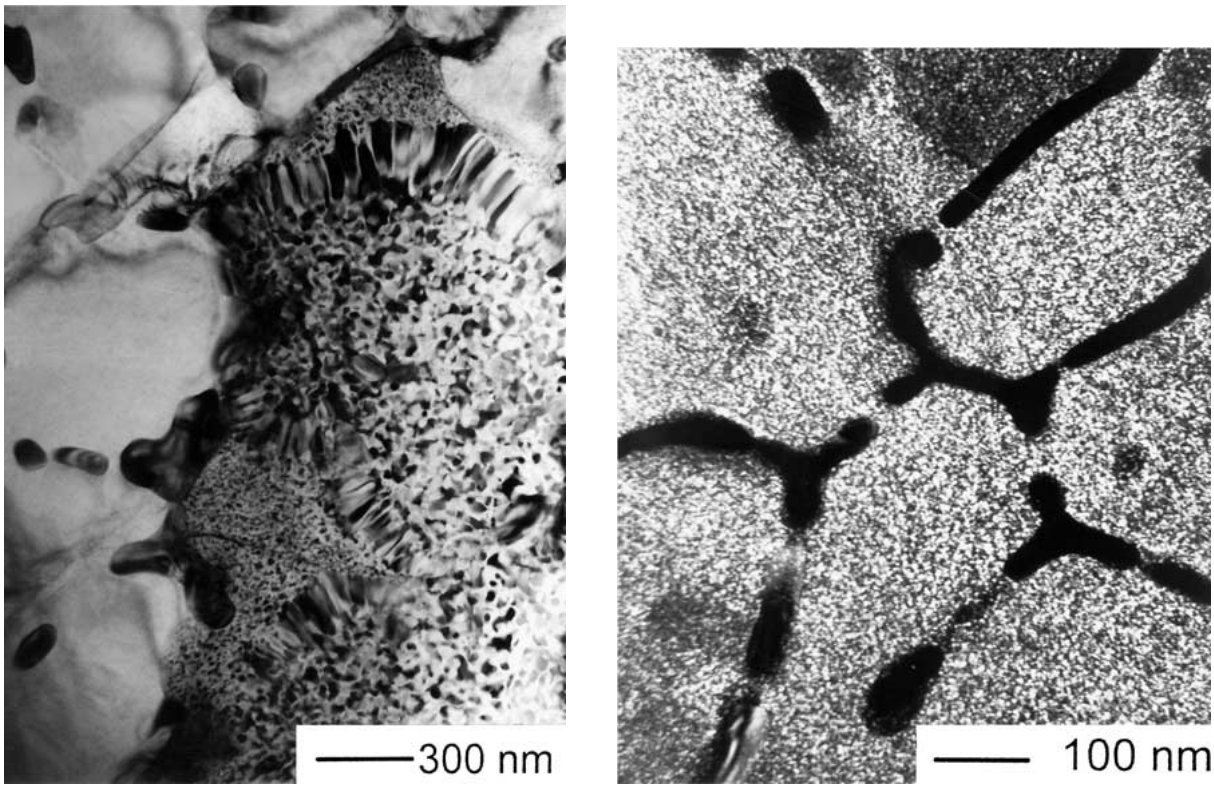

(a) (b)

Figure 7 Ti-25Al-2.5Si (at.%), melt spun at 30 m/s; (a) three different morphologies of APDs in the primary α_2 cells/dendrites, (BF g = 101) and (b) Ti-25Al-5Si (at.%), melt spun at 25 m/s; DF image obtained with $\alpha_2(101)$ superlattice reflection showing very fine APDs in the primary α_2-Ti_3(Al,Si) dendrites, TEM.

prependicular to the grain boundaries. Columnar (elongated) APDs adjacent to the grain boundaries in α_2-Ti_3Al based alloys have been observed previously by Ahmed [7], Munroe [8] and de Farias Azevedo and Flower [9]. Formation of elongated APBs at the α_2/B2 interfaces in Ti-Al-V alloys is related to the migration of the interface or the start of nucleation of ordered domains at the grain boundaries, [7]. De Farias Azevedo and Flower [9] observed columnar APBs in α_2-Ti_3(Al,Si) and concluded that the elongated domains were heterogeneously nucleated at certain α boundaries, as suggested by Williams [10]. Similar microstructural features have been noted in other alloy systems, e.g. Ni_2V [11], where nucleation of ordered domains occurs initially adjacent to grain boundaries, and then growth continues into the interior of grains by migration of the grain boundary leaving trails of APB's behind. The growth of such columnar APD's

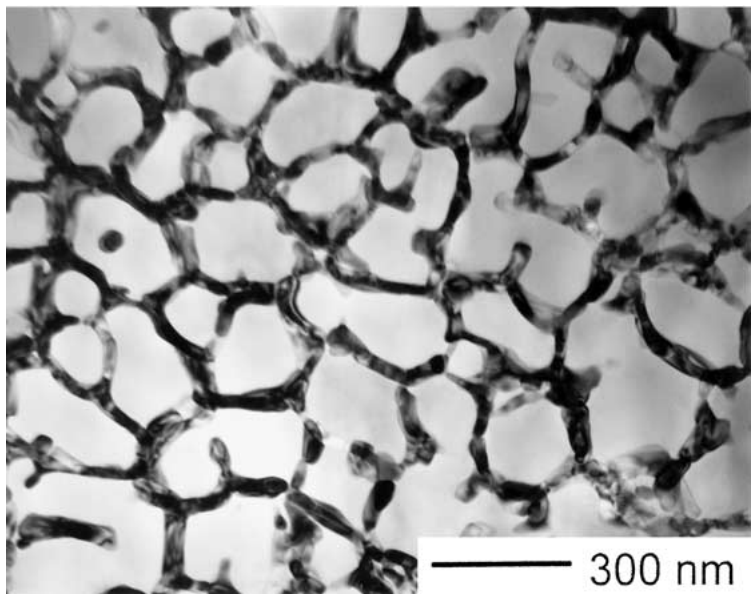

(a)

Figure 8 Ti-25Al-15V-5Si (at.%), melt spun at 30 m/s; (a) hypoeutectic structure. B2 cells/dendrites with inter-cellular/-dendritic ζ phase, BF image and (b) DF image on $(001)_{B2}$, showing APBs in the B2 cells/dendrites, TEM. (*Continued.*)

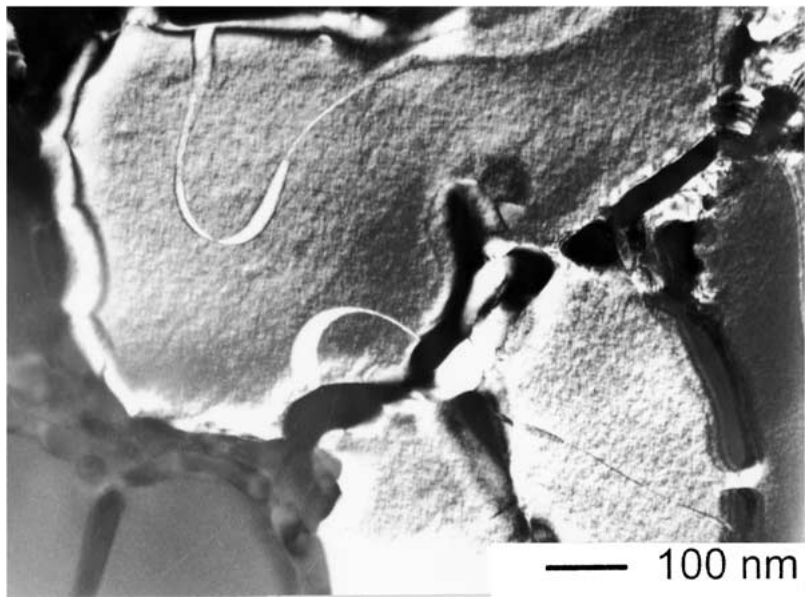

(b)

Figure 8 (*Continued*).

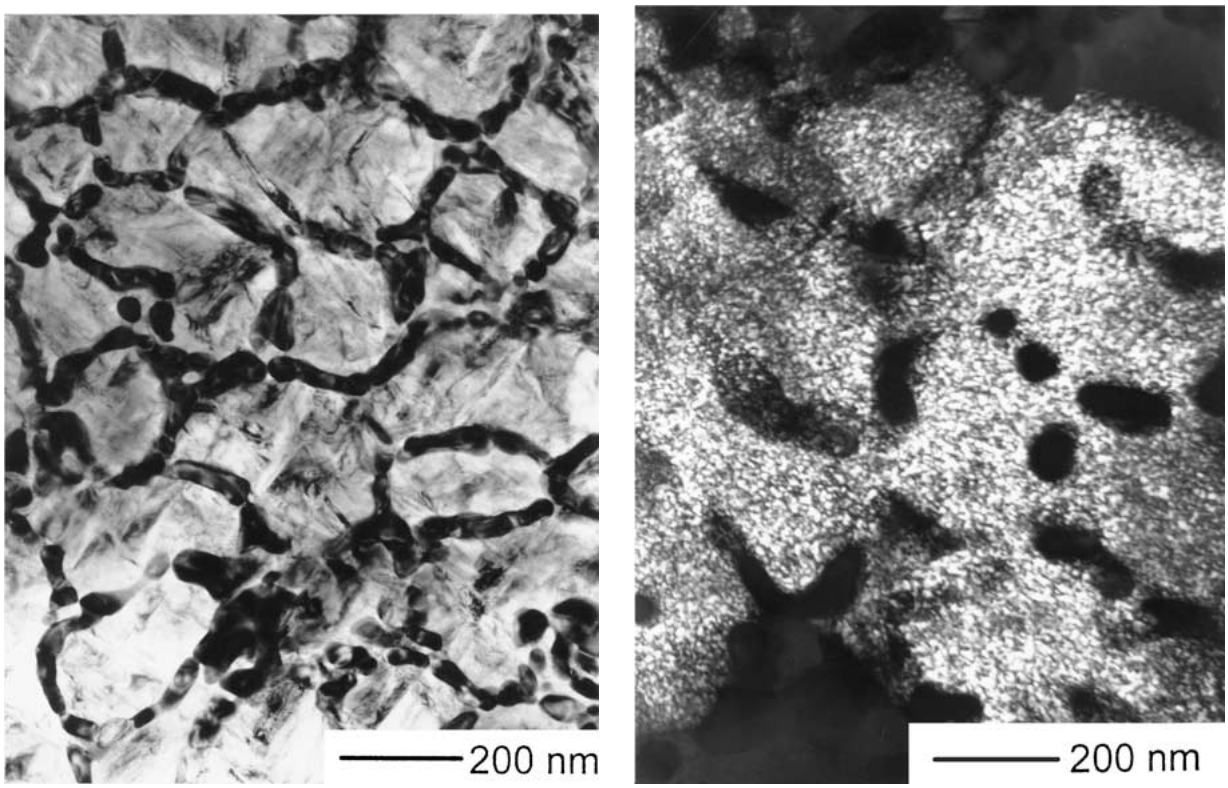

(a) (b)

Figure 9 Ti-25Al-7.5Si (at.%), melt spun at 30 m/s; (a) hypoeutectic structure, primary α_2-$Ti_3(Al,Si)$ dendrites with interdendritic ζ-$Ti_5(Si,Al)_3$ phase and (b) DF micrograph taken from the primary dendrites with $\alpha_2(101)$ superlattice reflection, showing fine APDs, TEM. (*Continued*.)

may be ultimately arrested by the development of homogeneously nucleated, equiaxed APD's within the grain interiors. The extent of each mechanism depends critically on local diffusion conditions and on the order/disorder transition temperature [12, 13]. Grain boundary diffusion normally dominates at lower temperatures with the possibility of formation of columnar APD's, whilst intragranular ordering is volume diffusion dependent and dominates in the higher temperature regimes, resulting in equiaxed APD's.

The observation of columnar antiphase domains near the grain boundaries in the present study suggests, therefore, that the ordering is initiated here by heterogeneous nucleation, with growth perpendicular to the grain boundaries. In contrast, the presence of an equiaxed APD structure in the grain interiors suggests that the domains nucleate homogeneously in these regions.

The formation of very fine antiphase domains adjacent to the grain boundaries in the α_2 phase in melt

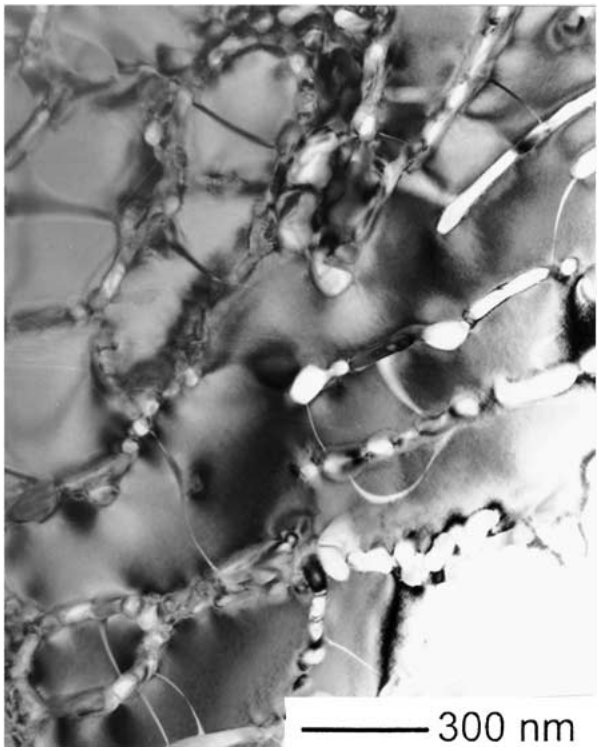

Figure 10 Ti-25Al-7.5Si-15V (at.%). Melt spun at 30 m/s; hypoeutectic structure, primary β-(Ti,V)(AL,Si) dendrites with interdendritic ζ-$Ti_5(Si,Al)_3$ phase. Coarse APDs in B2 phase. BF, $g = 001_{B2}$.

spun Ti-25Al and Ti-25 Al-2.5Si (at.%) ribbons is probably due to higher concentrations of impurity elements (especially oxygen) in these regions. It should be noted that these very fine antiphase domains are observed only in melt-spun Ti-25Al and Ti-25Al-2.5Si (at.%) alloys which contain higher oxygen concentrations (Table I).

Addition of 15 at.%V to Ti_3Al-based alloys leads to complete retention of the β phase at room temperature. This retained β phase, although stabilised with respect to the $\beta \rightarrow \alpha'$ martensitic transformation, is metastable with respect to other modes of decomposition and transforms to the ordered β phase during cooling [14]. Large antiphase domains observed in these alloys are characteristic of those that grow at relatively high temperatures.

5. Conclusions

The observation of a lath martensitic structure with fine antiphase domains in the primary α_2 cells/dendrites in melt-spun ribbons indicates that the prior bcc β cells/dendrites transform martensitically to the hcp α' phase because of the high cooling rate imposed by the melt spinning. This α' subsequently orders into the α_2 phase at lower temperatures.

The observation of columnar antiphase domains near the prior β grain boundaries and equiaxed APDs in the grain interiors in the arc-melted ingots suggests that the ordering occurs by both heterogeneous and homogeneous nucleation.

Addition of 15 at.%V to Ti_3Al-Si alloys lowers the $\beta \rightarrow \alpha$ transformation temperature and leads to complete retention of the ordered β phase at room temperature.

Acknowledgement

A. Jazayeri-G acknowledges financial support from Iranian Government.

References

1. H. A. LIPSITT, in Proc. Symp. 'High Temperature Ordered Intermetallic Alloys,' edited by C. C. Koch *et al*. (MRS, Pennsylvania, 1985) Vol. 39. p. 351.
2. Y. SUN, in "Intermetallic Compounds: Principles and Practice," edited by J. H. Westbrook *et al*. (John Wiley, Chichester, UK, 1995) p. 495.
3. J. R. BEELER, in "Intermetallic Compounds," edited by J. H. Westbrook (John Wiley, New York, 1967) p. 233.
4. H. A. LIPSITT, D. SHECHTMAN and R. E. SCHAFRIK, *Metall. Trans*. A **11A** (1980) 1369.
5. A. JAZAYERI-G, R. A. BUCKLEY and H. A. DAVIES, in Proc. Inst. Phys. Conf. Electron Microscopy and Analysis Group, EMAG99, 1999, Vol. 161, edited by C. J. Kiely, p. 471.
6. A. JAZAYERI-G, R. A. BUCKLEY and H. A. DAVIES, *Mater. Sci. and Tech*., in press.
7. T. AHMED, PhD thesis, Imperial College of Science, Technology and Medicine, London, 1992.
8. P. R. MUNROE, *Materials Forum* **17** (1993) 159.
9. C. R. DE FARIAS AZEVEDO and H. M. FLOWER, *Mater. Sci. Tech*. **15**(5) (1999) 510.
10. J. C. WILLIAMS, in "Titanium Technology: Present Status and Future Trends," edited by F. H. Froes *et al*. (The Titanium Development Association, Dayton, OH, 1985), p. 75.
11. L. E. TANNER, *Acta Met*. **20** (1972) 1197.
12. R. A. BUCKLEY, *Metal. Science* **9** (1975) 243.
13. M. RAJKOVIC and R. A. BUCKLEY, *Metal Science*. **15** (1981) 21.
14. D. BANERJEE, A. K. GOGIA, T. K. NANDY, K. MURALEEDHARAM and R. S. MISHRA, in Proc. 1st Inter. Symp. on Structural Intermetallics, edited by R. Darolia *et. al*. (TMS, Warrendale, 1993) p. 19.

Received 26 October 2001
and accepted 24 September 2002